Experimental Measurements of Rotordynamic Forces Caused by Front Shroud Pump Leakage

Robert V. Uy
Graduate Research Assistant.
e-mail: ruy@rand.org

Christopher E. Brennen
Professor.

Division of Engineering and Applied Science,
California Institute of Technology,
Pasadena, CA 91125

Unsteady forces generated by fluid flow through the impeller shroud leakage path of a centrifugal pump were investigated. Different pump shroud geometries were compared, and the effect of leakage path inlet swirl (pump discharge swirl) on the rotordynamic forces was examined for various ratios of fluid throughflow velocity to impeller tip speed. A short axial length leakage path reduced the measured forces, while curvature appeared to increase the destabilizing forces when inlet swirl was present. It was observed that changing the inlet swirl velocity does not appear to significantly affect the measured forces for a given leakage flow coefficient, but any nonzero inlet swirl is destabilizing when compared to cases with no inlet swirl.

Introduction

Previous experimental and analytical results have shown that discharge to suction leakage flows in the annulus surrounding a shrouded centrifugal pump contribute substantially to the fluid induced rotordynamic forces (Bolleter et al., 1987; Adkins and Brennen, 1988). Experiments conducted in the Rotor Force Test Facility (RFTF) at Caltech on an impeller undergoing a predetermined whirl motion have shown that the leakage flow contributions to the normal and tangential forces can be as much as 70% and 30% of the total, respectively (Jery, 1986). Other experiments have examined the consequences of leakage flows and have shown that the rotordynamic forces are functions not only of whirl ratio, but also of the leakage flow rate and the impeller shroud to pump housing clearance. The forces were found to be inversely proportional to the clearance. A region of forward subsynchronous whirl was found for which the average tangential force was destabilizing. This region decreased with increasing flow coefficient (Guinzburg et al., 1994).

Guinzburg et al. (1993) previously examined the difference in rotordynamic forces with and without a prescribed inlet swirl within the leakage path. The tangential force increased in the presence of inlet swirl, and hence the effect of inlet swirl was found to be destabilizing. Later studies by Sivo et al. (1995) examined the effectiveness of anti-swirl brakes in reducing the destabilizing region of forward whirl.

The present research examines differences between the conical leakage path, used by Guinzburg (1992, 1993, 1994) and Sivo (1994, 1995), and leakage paths with more typical geometry. A parametric evaluation of the effect of leakage path inlet swirl on the measured rotordynamic forces is also carried out.

Rotordynamic Forces

Figure 1 shows a schematic of the hydrodynamic forces that act on a rotating impeller whirling in a circular orbit. The unsteady fluid forces acting on the impeller due to the imposed whirl motion (eccentricity ϵ, whirl frequency Ω) are decomposed into a force normal to the direction of whirl motion, F_n, and a force in the direction of forward whirl motion, F_t. The normal and tangential forces are traditionally presented in dimensionless form as functions of the whirl frequency ratio, Ω/ω. More specifically, it is convenient for rotordynamicists to fit F_n to a quadratic function of the whirl frequency ratio, Ω/ω, and to fit the dimensionless tangential force, F_t, to a linear function. These expressions are:

$$F_n = M\left(\frac{\Omega}{\omega}\right)^2 - c\left(\frac{\Omega}{\omega}\right) - K \tag{1}$$

$$F_t = -C\left(\frac{\Omega}{\omega}\right) + k \tag{2}$$

where the dimensionless coefficients are the direct added mass (M), direct damping (C), cross-coupled damping (c), direct stiffness (K), and the cross-coupled stiffness (k). It should be noted that the fluid-induced forces may not always conform to these simple functions of the whirl frequency ratio. However, this assumption is common in the rotordynamics literature. Brennen (1994) and Jery (1986) contain more detailed discussions of the derivation of Eqs. (1) and (2), and the process for experimentally measuring the forces. All five of the force coefficients are directly evaluated from curve fits to the graphs of F_n and F_t against Ω/ω.

In considering rotor stability, a positive normal force F_n will cause the eccentricity to increase and hence be destabilizing. From Eq. (1), a large negative direct stiffness when no whirl motion is present ($\Omega/\omega = 0$) would correspond to such a case. When Ω/ω is positive, a positive tangential force F_t would also be destabilizing as this would drive the forward whirl motion.

A convenient measure of the rotordynamic stability is the ratio of cross-coupled stiffness to the direct damping (i.e., k/C) which is termed the whirl ratio. This defines the range of positive whirl frequency ratios, $0 < \Omega/\omega < k/C$, for which the tangential force is destabilizing.

Figure 2 shows the rotordynamic forces for different flow coefficients as functions of the whirl frequency ratio. A quadratic curve fit for F_n appears appropriate with little loss in accuracy; however a linear fit for F_t would seem to provide an adequate but approximate model of the tangential force.

The magnitude of the forces presented in this study confirm the significance of the shroud forces to the overall rotordynamic forces. For example, Jery (1986) reports stiffnesses for Impeller X/Volute A at design flow of $K = -2.61$ and $k = 1.12$, while using data for $\phi = .009$ in Fig. 2, $K = -.42$ and $k = .62$. Multiplying these by the nondimensionalizing force in both cases, $K = -9.3$ KN/m and $k = 3.99$ KN/m for Jery's tests, while $K = -5.37$ KN/m and $k = 7.92$ KN/m for the current tests. The forces appear to be of similar magnitude, despite significant differences in the geometry and clearance. It is also worth noting that the whirl ratio, k/C, is similar to tests conducted by Jery, but smaller than that reported by Bolleter et al. (1987). Large differences in the

Contributed by the Fluids Engineering Division for publication in the JOURNAL OF FLUIDS ENGINEERING. Manuscript received by the Fluids Engineering Division; revised manuscript received May 15, 1999. Associate Technical Editor: B. Schiavello.

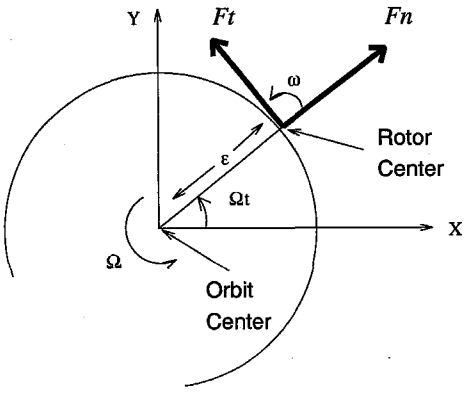

Fig. 1 Schematic of the fluid induced forces acting on an impeller whirling in a circular orbit

leakage path geometry exist between Bolleter and the current tests, most notably in the suction side geometry. The differences in rotordynamic behavior between axial clearance and radial clearance low pressure seals is detailed in Uy et al. (1998).

Test Apparatus

The present experiments were conducted in the Rotor Force Test Facility (RFTF) at Caltech (Jery, 1986). The leakage flow test section of the facility is schematically shown in Figs. 3 and 4. The intention is to isolate the leakage flow forces by using a solid rotor and to generate the flow through the leakage path by an auxiliary pump. The main components of the test section apparatus consist of the solid rotor, a stator (the stationary shroud), the rotating dynamometer (or internal force balance), an eccentric whirl mechanism and a leakage exit seal ring. The working fluid is water. An inlet guide vane is used for the tests with fluid prerotation and appears in Fig. 4.

The rotor is mounted directly to the rotating dynamometer, which in turn is connected to a data acquisition system that permits measurements of the rotordynamic force matrix components (Jery, 1986). The eccentric drive mechanism imposes a circular whirl orbit on the basic main shaft rotation. The radius of the whirl orbit (eccentricity) can be varied but this set of experiments used one eccentricity, $\epsilon = 0.025$ cm. The seal ring at the leakage exit models a wear ring. The clearance between the face seal and the impeller face is adjustable.

The temperature drift of the dynamometer electronics is postulated to be the largest contributor to force measurement errors. The uncertainty in all reported rotordynamic force coefficients is 5% with the exception of the direct stiffness, K, for which the uncertainty is 8%. The uncertainty in the measurement of the flow rate is 1%.

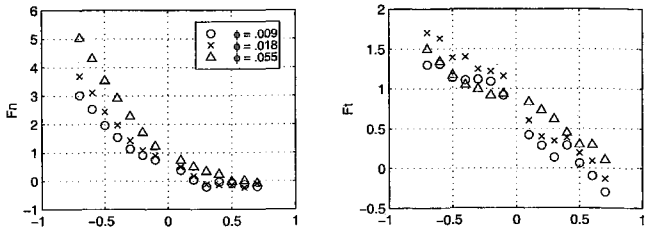

Fig. 2 Experimental rotordynamic forces plotted versus whirl frequency ratio Ω/ω, for indicated flow coefficients

The experimental configurations with the rotor and stator forming the leakage path, are shown in Fig. 3. The conical rotor and shroud with the straight 45 degree leakage path have been extensively tested previously by Guinzburg and Sivo. The contoured rotor was made to match the axial length and eye-to-tip ratio (the ratio of an impeller's inlet diameter to the discharge diameter) of the conic model, but have more typical geometry. The third rotor and stator were made to model the leakage path of the Space Shuttle Main Engine (SSME) High Pressure Oxidizer Turbopump (HPOTP) as closely as possible. It was much shorter in axial length than the previous two impellers and had a much larger eye radius. Both contoured rotors were designed using a third-order polynomial chosen such that the contour was parallel to the centerline at the eye and perpendicular to the centerline at the tip. A matching stator was constructed to maintain a constant clearance, $H = 0.30$ cm, normal to the surfaces of the rotor and stator. The tip radius (corresponding to the discharge radius of a pump) of all of the rotors is the same.

The effect of inlet swirl was investigated by installing guide vanes at the leakage inlet to introduce pre-rotation in the direction of shaft rotation. Figure 4 shows a typical vane consisting of a logarithmic spiral channel with a turning angle of 6 degrees. A series of vanes with angles $\alpha = 1$, 2, and 6 deg were fabricated. The swirl ratio, Γ (the ratio of the leakage flow circumferential velocity to the impeller tip velocity) is varied by changing the inlet leakage flow rate and the turning angle. The swirl ratio depends on the flow coefficient and turning angle according to:

$$\frac{\Gamma}{\phi} = \frac{H}{B \tan \alpha} \tag{3}$$

Nomenclature

B = width of logarithmic spiral channel and swirl vane
C = direct damping coefficient, normalized by $\rho\pi\omega R_2^2 L$
c = cross-coupled damping coefficient, normalized by $\rho\pi\omega R_2^2 L$
F_n = force normal to whirl orbit normalized by $\rho\pi\omega^2 R_2^2 L\epsilon$
F_t = force tangent to whirl orbit normalized by $\rho\pi\omega^2 R_2^2 L\epsilon$
H = normal clearance between impeller shroud and housing
K = direct stiffness coefficient, normalized by $\rho\pi\omega^2 R_2^2 L$
k = cross-coupled stiffness coefficient, normalized by $\rho\pi\omega^2 R_2^2 L$
k/C = whirl ratio, a measure of the destabilizing region of F_t
L = axial length of the leakage path
M = direct added mass coefficient, normalized by $\rho\pi R_2^2 L$
Q = volumetric leakage flow rate
R_2 = radius of rotor and leakage path inlet, in these experiments, 9.366 cm
Re_ω = Reynolds number based on rotational speed, $R_2\omega H/\nu$
Re_{u_s} = Reynolds number based on fluid through velocity, $u_s H/\nu$
Re_{u_θ} = Reynolds number based on fluid rotational velocity, $u_\theta H/\nu$
u_s = mean throughflow velocity of fluid at the leakage path inlet, $Q/2\pi R_2 H$
u_θ = mean swirl velocity of fluid at the leakage path inlet
α = angle of logarithmic spiral swirl vane
Γ = leakage inlet swirl ratio, $u_\theta/\omega R_2$
ϵ = eccentricity of whirl orbit
ν = kinematic viscosity
ρ = fluid density
ϕ = leakage flow coefficient, $u_s/\omega R_2$
ω = main shaft radian frequency
Ω = whirl radian frequency
Ω/ω = whirl frequency ratio

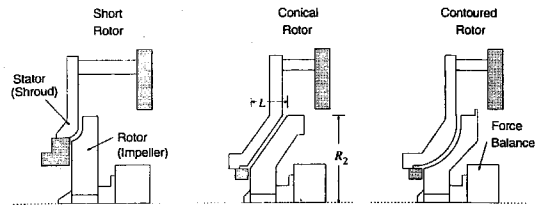

	Short Rotor	Conical Rotor	Contoured Rotor
Path	3rd order	45 degree	3rd order
Eye/tip diameter	.700	.474	.474
Axial length/ tip diameter	.088	.268	.229
L (cm)	1.65	5.02	4.29

Fig. 3 Test matrix of rotor geometries (see Fig. 4 for more detail). Configurations are symmetric about the centerline.

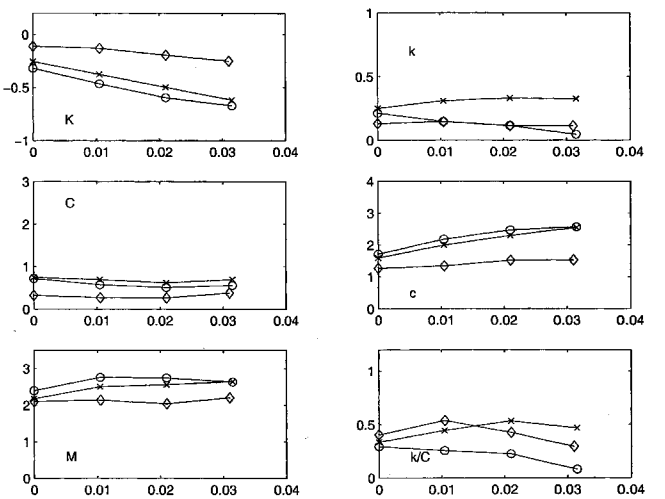

Fig. 5 Experimental rotordynamic coefficients versus flow coefficient, ϕ, for the conical (○), contoured (×), and short (◇) leakage paths ($\Gamma = 0$)

where $B = 0.318$ cm is the width of the logarithmic spiral channel. A derivation of Eq. (3) (which assumes all leakage flow is constrained to follow the vane) is found in Guinzburg et al. (1993). In the present tests it was possible to examine the variation of the forces with α or ϕ while maintaining the same Γ.

Effect of Path Shape

Variations in leakage path geometry were examined using the rotors (dummy impellers) and stators described in the previous section. The conical rotor and stator were tested and compared to the contoured rotor and stator with the same eye diameter, tip diameter, axial length, and leakage path clearance. Results for the short rotor/stator combination are also compared. For these comparisons, a constant main shaft speed, ω, of 1000 rpm was used. A range of leakage flow coefficients from 0 to .033 were studied using flow rates of 0, .19, .37, and .57 l/s; these span the range of leakage flow rates in many industrial applications. The Reynolds numbers for $\phi = .033$ would be $\mathrm{Re}_\omega = 27177$ and $\mathrm{Re}_{u_s} = 896$. A constant leakage path clearance of $H = .30$ cm was also used in comparative tests. The rotordynamic force coefficients were derived from a least squares quadratic and linear fit of the normal and tangential forces, respectively, F_n and F_t, which were measured over the range of whirl frequency ratios, $-0.7 < \Omega/\omega < 0.7$. Figure 5 presents the dimensionless rotordynamic force coefficients as functions of the leakage flow coefficient, and compares the conical and contoured leakage path geometries. In these tests, no guide vane was used and the inlet swirl ratio, Γ, is assumed to be zero.

Except for the cross-coupled stiffness, k, all of the rotordynamic force coefficients are similar (in both trend and magnitude) for the contoured and conical rotors. Thus, the effect of the geometry of the passage is relatively small provided that parameters such as the eye/tip diameter and axial length are the same. The effect of a shorter path length, (which alters the nondimensionalization due to the axial length) with a larger eye/tip diameter ratio, is also clear when all three geometries are compared. The forces for this short rotor are much smaller in magnitude. The coefficients K, c, M, are virtually identical for the conical and contoured geometries, reflecting the fact that the path shape has little effect on the dimensionless normal force, F_n. The normal force coefficients for the short rotor follow the same trends as the other two leakage paths, but are smaller in magnitude across the entire range of flow coefficients.

The contoured rotor has a larger cross-coupled stiffness, k, than the conical rotor over the entire whirl frequency range. The cross-coupled stiffness for the short rotor follows the same trend as the contoured impeller, but with a smaller magnitude. The direct damping, C, seems to be fairly uniform for all three rotors, with the short rotor showing a slightly smaller magnitude. The change in k produces a corresponding change in the whirl ratio, k/C.

Earlier, it was reported by Guinzburg (1992) and Sivo (1995), that, with the conical geometry, the whirl ratio decreased with increasing flow coefficient, and this is confirmed in the present experiments with the conical geometry. However, the contoured geometry produces a k/C which increases with increasing flow coefficient. This trend may reverse at higher flow coefficients (as suggested by the fact that the short rotor exhibits a whirl ratio, k/C, which decreases with ϕ). Indeed, in the tests with inlet swirl described in the next section, the contoured path was subjected to much larger flow rates and the whirl ratio decreased at larger values of ϕ than are shown in this section.

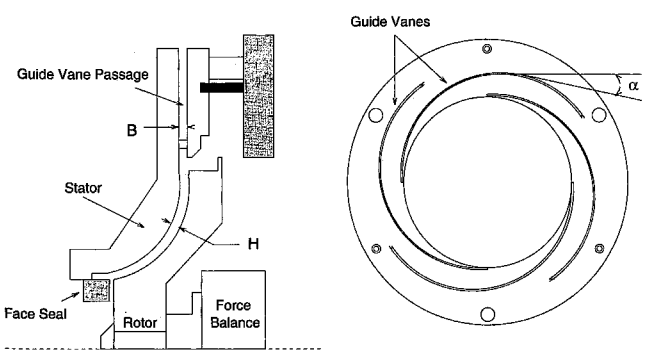

Fig. 4 Inlet guide vane, 6 degree turning angle

Effect of Inlet Swirl

A set of experiments was also carried out to determine the effect of inlet swirl on the unsteady rotordynamic forces in the contoured leakage path. The three swirl vanes of different turning angles were employed to alter the inlet swirl ratio, and a swirl vane with perpendicular channels, ($\alpha = 90$ deg), was used to generate data for zero inlet swirl. In this case, the flow coefficient ranges from $\phi = 0.01$ to 0.066 using flow rates from .17 to 1.15 l/s. The Reynolds numbers for $\phi = .055$ and $\Gamma = .5$ would be $\mathrm{Re}_\omega = 27177$, $\mathrm{Re}_{u_s} = 1494$ and $\mathrm{Re}_{u_\theta} = 13588$. Figure 6 presents plots of the dimensionless rotordynamic force coefficients obtained from the swirl experiments as functions of the leakage flow coefficient. It appears as though the inlet swirl, Γ, has little effect on the forces for any flow rate. However, the effect of swirl is destabilizing compared to the case with no swirl, as K has a larger negative magnitude and k/C is increased. This was previously observed by Guinzburg (1992).

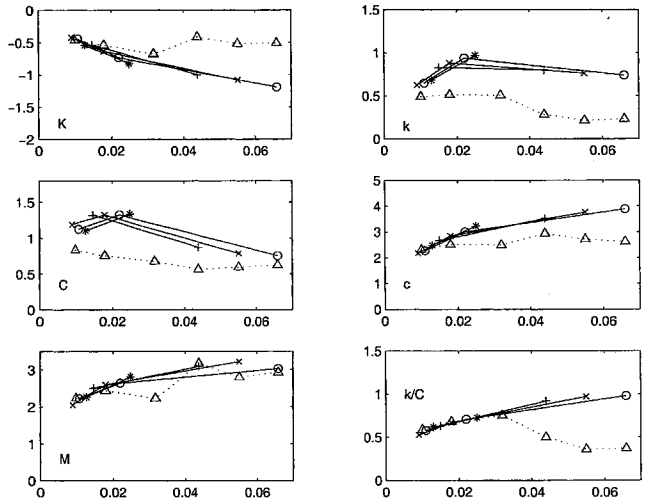

Fig. 6 Experimental rotordynamic coefficients plotted against flow coefficient, ϕ, for tests with inlet swirl, Γ = 0.0 (△), 0.4 (+), 0.5 (×), 0.6 (○), and 0.7 (*), contoured leakage path

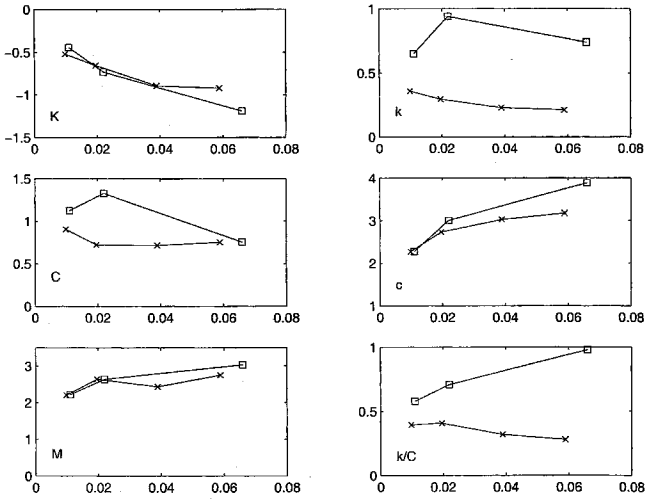

Fig. 7 Experimental rotordynamic coefficients plotted against flow coefficient ϕ for tests with inlet swirl, for the contoured leakage path (□, Γ = .6), and for the conical leakage path (×, Γ variable)

The tangential force coefficients, C and k, are larger when swirl is present than in the absence of inlet swirl. The cross-coupled stiffness with inlet swirl remains at an almost constant level for various values of Γ, while the direct damping shows a tendency to first increase and then decrease slightly with increasing flow coefficient. This leads to a whirl ratio, k/C, that increases with increasing flow coefficient. In the case with no swirl, however, a reduction of the whirl ratio is observed for the contoured dummy impeller at higher flow rates. Some difference in k may be noted between the tests with the 90 deg inlet guidevane and the tests in Fig. 5, where the swirl, Γ, was assumed zero. Clearly the tangential force is highly sensitive to the leakage path inlet conditions, and this discrepancy would indicate that in the cases with no inlet guidevanes present, some pre-rotation of the fluid may be occuring before it enters the leakage path.

Upon examination of the coefficients which determine the normal force, the same trends for M, c, and K observed for the conical rotor by Guinzburg and Sivo are also seen in the present experiments. The added mass does not exhibit an appreciable difference in the cases with and without swirl, but the magnitude of the direct stiffness is higher and the magnitude the cross-coupled damping is smaller with no inlet swirl. In summary, the circumferential fluid velocity induced by inlet swirl affects the rotordynamic behavior significantly if it is nonzero, but the amount of prerotation, Γ, has little influence on the rotordynamics.

The combined effect of inlet swirl and leakage path geometry was also investigated. Figure 7 presents the rotordynamic force coefficients for both the contoured and conical leakage path geometry. The coefficients of the normal force appear to be similar, but there are significant differences in the trend and magnitude of the cross-coupled stiffness and direct damping, leading to substantial differences in the whirl ratio. The contoured rotor exhibits an increasing trend with flow rate, while the conical rotor indicates a decreasing trend.

Discussion and Summary

The experimental data from the current research shows good agreement with previous work in the area of fluid-induced rotordynamic forces in pump leakage paths. The functional dependence of the forces on whirl frequency ratio, Ω/ω, was fairly consistent and allowed quadratic fits to the data and therefore use of conventional rotordynamic force coefficients for meaningful comparisons. Particular attention was paid to the variation in the whirl ratio, k/C, with flow coefficient and with other geometric parameters.

Different leakage path geometries were investigated to evaluate the effects of the front shroud geometry on the forces. A reduced axial length decreases the magnitude of all the rotordynamic force coefficients. As the forces are nondimensionalized by the axial length, this implies that the forces are quite small for the shorter contoured rotor, and that the nondimensionalization with the axial length will not reduce the forces on the rotors with similar profiles to uniform values. The effect of the shroud curvature on rotors of similar axial length was also examined. Only the cross-coupled stiffness for the case with no swirl seems to be affected by the curvature, but both tangential force coefficients, C and k, are affected in the case with inlet swirl. The whirl ratio decreases with increasing throughflow as previously observed for the conical geometry. There are indications that this also occurs with contoured rotors, but at much higher flow rates.

The tests with inlet swirl, Γ, indicate significant fluid effects on the forces. The direct stiffness, direct damping, and cross-coupled stiffness show the greatest change between cases with and without inlet swirl. The magnitude of the fluid pre-rotation, Γ, into the path does not appear to be an important factor on the measured forces. It is postulated that the effect of inlet swirl is largest only at the inlet to the leakage path, and that the viscous effects dominate thereafter. Inlet swirl seems to have very different effects on the tangential force for the conic and contoured geometries, and appears to be more destabilizing with increasing flow rate for the case with curvature.

Concluding Remarks

The effect of front shroud geometry on the rotordynamic forces in shrouded centrifugal pumps has been investigated. Experimental results suggest several options for designers of pumping machinery where fluid-induced rotordynamic forces may be encountered. The short axial length rotor with a larger eye radius experienced rotordynamic forces which were much smaller in magnitude than the longer rotors. Curvature of the leakage path increases the region of forward whirl where the tangential force is destabilizing, and this effect is even more pronounced if inlet swirl is present. The amount of inlet swirl is not a significant factor, but its effect is to increase the magnitude of the rotordynamic forces. Thus, measures to reduce the amount of swirl entering the leakage path may aid stability.

In order to place all of the effects of geometry, inlet swirl, etc., in the context of a coherent prediction methodology, we are currently developing a bulk-flow model which we believe will add to our understanding of the reasons behind many of these fluid mechanical phenomena. The development of this model and the results it yields will be presented in a later companion paper.

Acknowledgments

The authors wish to thank the Advanced Rotating Machinery group of Rocketdyne division of Rockwell Aerospace for financial support and assistance.

References

Adkins, D., and Brennen, C., 1988, "Analysis of Hydrodynamic Radial Forces on Centrifugal Pump Impellers," ASME JOURNAL OF FLUIDS ENGINEERING, Vol. 110, No. 1, pp. 20–28.

Bolleter, U., Wyss, A., Welte, I., and Sturchler, R., 1987, "Measurement of Hydraulic Interaction Matrices of Boiler Feed Pump Impellers," ASME *Journal of Vibrations, Stress, and Reliability in Design,* Vol. 109, pp. 144–151.

Brennen, C., 1994, *Hydrodynamics of Pumps.* Concepts ETI and Oxford University Press.

Guinzburg, A., 1992, "Rotordynamic Forces Generated By Discharge-to-Suction Leakage Flows in Centrifugal Pumps," Ph.D. thesis, California Institute of Technology.

Guinzburg, A., Brennen, C., Acosta, A., and Caughey, T., 1993, "The Effect of Inlet Swirl on the Rotordynamic Shroud Forces in a Centrifugal Pump," ASME *Journal of Engineering for Gas Turbines and Power,* Vol. 115, No. 2, pp. 287–293.

Guinzburg, A., Brennen, C., Acosta, A., and Caughey, T., 1994, "Experimental Results for the Rotordynamic Characteristics of Leakage Flows in Centrifugal Pumps," ASME JOURNAL OF FLUIDS ENGINEERING, Vol. 116, No. 1, pp. 110–115.

Jery, B., 1986, "Experimental Study of Unsteady Hydrodynamic Force Matrices on Whirling Centrifugal Pump Impellers," Ph.D. thesis, California Institute of Technology.

Sivo, J., Acosta, A., Brennen, C., and Caughey, T., 1995, "The Influence of Swirl Brakes on the Rotordynamic Forces Generated by Discharge-to-Suction Leakage Flows in Centrifugal Pumps," ASME JOURNAL OF FLUIDS ENGINEERING, Vol. 117, No. 1, pp. 104–108.

Tsujimoto, Y., Yoshida, Y., Ohashi, H., and Ishizaki, S., 1997, "Fluid Force Moment on a Centrifugal Impeller in Precessing Motion," ASME JOURNAL OF FLUIDS ENGINEERING, Vol. 119, No. 2, pp. 366–371.

Uy, R., Bircumshaw, B., and Brennen, C., 1998, "Rotordynamic Forces from Discharge-to-Suction Leakage Flows in Shrouded Centrifugal Pumps: Effects of Geometry," *JSME International Journal: Fluids and Thermal Engineering,* Vol. 41, No. 1, pp. 208–213.